NACA TN 2657

NATIONAL ADVISORY COMMITTEE FOR AERONAUTICS

TECHNICAL NOTE 2657

SOME EFFECTS OF FREQUENCY ON THE CONTRIBUTION OF A VERTICAL TAIL TO THE FREE AERODYNAMIC DAMPING OF A MODEL OSCILLATING IN YAW

By John D. Bird, Lewis R. Fisher,
and Sadie M. Hubbard

Langley Aeronautical Laboratory
Langley Field, Va.

NACA
Washington
April 1952

ERRATA NO. 1

NACA TN 2657

SOME EFFECTS OF FREQUENCY ON THE CONTRIBUTION OF A VERTICAL TAIL TO THE FREE AERODYNAMIC DAMPING OF A MODEL OSCILLATING IN YAW

By John D. Bird, Lewis R. Fisher,
and Sadie M Hubbard

April 1952

Errors in sign and the omission of the factor 2 in certain of the equations on pages 21 and 22 should be corrected as follows:

Page 21: First equation should be:

$$Y(\alpha,h) = \frac{\rho c_t^2}{4}\left(V\pi\dot{\alpha} + \pi\ddot{h} - \frac{\pi c_t a\ddot{\alpha}}{2}\right) + \pi\rho V c_t C(k)\left[V\alpha + \dot{h} + \frac{c_t}{2}\left(\frac{1}{2} - a\right)\dot{\alpha}\right]$$

Last two equations should be:

$$Y(\beta) = -qc_t\,\frac{\pi}{2}\left[c_t\left(\frac{\dot{\beta}}{V}\right) + 4C(k)\beta\right]$$

$$Y(\psi) = qc_t^2\,\frac{\pi}{2}\left[2C(k)\left(\frac{1}{2} - a\right)\frac{\dot{\psi}}{V} - \frac{c_t}{2}\,a\,\frac{\ddot{\psi}}{V^2}\right]$$

NATIONAL ADVISORY COMMITTEE FOR AERONAUTICS

TECHNICAL NOTE 2657

SOME EFFECTS OF FREQUENCY ON THE CONTRIBUTION OF A VERTICAL TAIL TO THE FREE AERODYNAMIC DAMPING OF A MODEL OSCILLATING IN YAW

By John D. Bird, Lewis R. Fisher, and Sadie M. Hubbard

SUMMARY

The directional damping and stability of a fuselage - vertical-tail model oscillating freely in yaw were measured at a Mach number of 0.14 and compared with the damping and stability obtained by consideration of the effects of unsteady lift. The contribution of the vertical tail to the damping in yaw of the model agreed within the limits of experimental accuracy with predictions of the approximate finite-aspect-ratio unsteady-lift theories for the range of frequencies tested, and the two-dimensional unsteady-lift theory predicted a much greater loss in damping with reduction in frequency than was shown by experiment or by the approximate finite-aspect-ratio unsteady-lift theories. For frequencies comparable to those of lateral airplane motions, both the unsteady-lift theories and the experimental results indicated that the contribution of the vertical tail to the directional stability of the model was relatively independent of frequency.

INTRODUCTION

The advent of high-speed airplanes of high relative density has focused attention on certain problems associated with the dynamic stability of airplanes which, because of previous unimportance, have heretofore been neglected. Among these problems is the effect of the periodicity of the airplane motion on the effective values of the various stability derivatives. Reference 1 and, more recently, references 2 and 3 have indicated the possibility of sizeable effects from this problem.

An appreciable amount of theoretical work on these unsteady-lift effects exists at present; however, only a small amount of experimental substantiation of the results is available for the low-frequency range of oscillation. As a result a program has been undertaken in the

Langley stability tunnel to determine the effects of such variables as frequency and amplitude of motion on the contribution of the various airplane components to the stability derivatives of present-day airplane configurations. The work reported herein covers that phase of the investigation which considers frequency effects on the directional damping and stability of a model undergoing a freely damped oscillatory yawing motion. The effects of vertical-tail aspect ratio and compressibility as predicted by the theoretical treatments are discussed in relation to the experimental stability characteristics obtained by the free-oscillation and by the curved-flow procedures.

SYMBOLS

The data are referred to the system of stability axes and are presented in the form of standard NACA coefficients of forces and moments about the quarter-chord point of the mean aerodynamic chord of the normal wing location of the model tested. (See fig. 1.) The coefficients and symbols used herein are defined as follows:

C_L	lift coefficient (L/qS_w)
C_D	drag coefficient (D/qS_w)
C_Y	lateral-force coefficient (Y/qS_w)
C_l	rolling-moment coefficient (L'/qS_wb_w)
C_m	pitching-moment coefficient $(M/qS_w\bar{c}_w)$
C_n	yawing-moment coefficient (N/qS_wb_w)
L	lift, pounds
D	drag, pounds
Y	lateral force, pounds
L'	rolling moment, foot-pounds
M	pitching moment, foot-pounds
N	yawing moment, foot-pounds
q	dynamic pressure, pounds per square foot $\left(\frac{1}{2}\rho V^2\right)$

ρ	mass density of air, slugs per cubic foot
V	free-stream velocity, feet per second
S	area, square feet
b	span, feet
c	chord, feet
c_t	mean tail chord, feet
$\bar{c}$	mean aerodynamic chord, feet $\left(\frac{2}{S}\int_0^{b/2} c^2 dy\right)$
y	spanwise distance from the plane of symmetry
A	aspect ratio (b^2/S)
α	angle of attack, degrees
β	angle of sideslip, radians
$\dot{\beta} = \frac{d\beta}{dt}$	
t	time, seconds
$\frac{rb}{2V}$	yawing-velocity parameter
ψ	angle of yaw, radians
$r, \dot{\psi}$	yawing velocity, radians per second $(d\psi/dt)$
$\dot{r}, \ddot{\psi}$	yawing acceleration, radians per second per second $\left(d^2\psi/dt^2\right)$
ω	angular velocity, radians per second
f	frequency, cycles per second
k	reduced-frequency parameter referred to semichord of vertical tail $(\omega c_t/2V)$
N_ψ	mechanical spring constant, foot-pounds per radian

I_Z yawing moment of inertia, foot-pound-second^2

$t_{1/2}$ time to damp to one-half amplitude, seconds

m damping constant

P period of oscillation, seconds

a nondimensional tail length referred to semichord of vertical tail $\left(-\frac{l}{c_{t/2}}\right)$

l distance from origin of axes to midchord point of vertical tail, feet

$C(k) = F + iG$

F,G circulation functions used by Theodorsen (reference 6)

$\overline{P} = F + iG$
$\overline{Q} = H + iJ$
finite-span functions used by Biot and Boehnlein (reference 9)

σ finite-span correction used by Reissner (reference 8)

Z,M compressible-flow functions used in place of F and G (references 10 and 11)

A,B functions of k defined in text

$$C_{n_r} = \frac{\partial C_n}{\partial \frac{rb}{2V}}$$

$$C_{n_{\dot{r}}} = \frac{\partial C_n}{\partial \frac{\dot{r}b^2}{4V^2}}$$

$$C_{Y_r} = \frac{\partial C_Y}{\partial \frac{rb}{2V}}$$

$$C_{n_\beta} = \frac{\partial C_n}{\partial \beta}$$

$$C_{n_{\dot{\beta}}} = \frac{\partial C_n}{\partial \frac{\dot{\beta} b}{2V}}$$

$$C_{Y_\beta} = \frac{\partial C_Y}{\partial \beta}$$

$$N_{\dot{\psi}} = \frac{\partial N}{\partial \dot{\psi}}$$

$$N_{\ddot{\psi}} = \frac{\partial N}{\partial \ddot{\psi}}$$

$$N_\beta = \frac{\partial N}{\partial \beta}$$

$$N_{\dot{\beta}} = \frac{\partial N}{\partial \dot{\beta}}$$

Subscripts:

w	wing
t	vertical tail
o	amplitude
f	due to friction

APPARATUS

Model and Oscillating Strut

The model used in this investigation and shown in figure 2 had separable wing, fuselage, and tail surfaces and was constructed almost

entirely of balsa wood in order to minimize the mass and make the natural frequency of the model on its mounting as high as possible. The configuration is representative of that of several present-day high-speed airplanes. The aspect ratio A and mean chord c_t of the vertical tail were 2 and 4.9 inches, respectively.

The model was mounted at the quarter chord of the wing mean aerodynamic chord on a 1-inch-diameter rod which rotated with respect to a circular hollow strut and which was connected to it by means of flexure pivots made of Swedish steel. Flexure pivots were used rather than bearings in order to minimize the friction in the system. The pivots were alined with the center of the rod on which the model was mounted. The entire assembly, which is shown in figures 3 and 4, was fastened to the ceiling of the tunnel test section and covered by a streamlined fairing.

The inner rod or oscillating strut, which was permitted to rotate and upon which the model was mounted, extended through the ceiling of the tunnel test section and was capped by a horizontal crosspiece. The period of oscillation of the model was controlled by varying the moment of inertia about the vertical axis of the system. This variation was accomplished by using crosspieces of different lengths and by clamping weights at the ends of the crosspieces.

Recording Device

A continuous record of the displacement in yaw of the model was made on photographic film by means of an optical recording system. A mirror clamped to the section of the oscillating strut which extended outside the tunnel reflected a beam of light from a point light source within the recorder. The beam was focused on a roll of photographic film by means of an 8-inch-focal-length double-concave lens. The film roll was driven at constant speed by gearing it to an electric motor. A 10-cycle-per-second neon timing light incorporated in the recorder exposed timing lines on the film in order that time as well as model displacement could be measured accurately on the film record.

TESTS

Oscillation Tests

The free-damping tests were conducted with the model in an inverted position, in order to minimize strut interference effects, and at zero angle of attack with respect to the fuselage reference line. The tests were conducted on the combination of fuselage and tail surface and on

the fuselage alone because preliminary tests had shown that the presence of the wing had no apparent effect on the damping at zero angle of attack. The range of moments of inertia and frequencies covered are shown together with the test results in table I. Results of runs made with wind on and off are given in order to illustrate the magnitude of the tares applied.

When tests were made of the fuselage alone, a torque rod was employed to provide a stable restoring moment to the fuselage which was equal to the aerodynamic moment provided by the vertical tail when attached. The torque rod was clamped between the extended oscillating strut and a building structural member as shown in figure 3. The spring constant of the system was 6.8 foot-pounds per radian for the flexure pivots alone and 32.8 foot-pounds per radian for the combination of the flexure pivots and the torque rod.

Force Tests

The steady-state stability characteristics of the model were determined through an angle-of-attack range from 0° to 8° for the fuselage alone, the fuselage and tail surfaces, and the complete configuration by means of wind-tunnel force tests. The model was mounted on a single-strut support and all forces and moments were measured by a six-component balance system. The steady-state sideslipping derivatives were determined through a sideslip range of $\pm 5^\circ$, and the yawing derivatives, at values of the yawing-velocity parameter $rb/2V$ of 0, -0.0291, -0.0616, and -0.0810 by standard stability-tunnel curved-flow testing procedures.

All tests were conducted in the 6- by 6-foot test section of the Langley stability tunnel at a dynamic pressure of 24.9 pounds per square foot, a Mach number of about 0.14, and a Reynolds number of 442,000 based on the wing mean aerodynamic chord. Standard jet-boundary corrections have been applied to the angle-of-attack, the drag-coefficient, and the rolling-moment-coefficient data obtained from the force tests. In addition, the steady-state yawing data have been corrected for the effects of the lateral static-pressure gradient peculiar to the curved-flow testing procedure. Jet-boundary corrections were not applied to the oscillation tests because of their insignificance for the test conditions involved. See reference 4.

REDUCTION OF OSCILLATION TEST DATA

From the continuous film record taken of the motion of the model after an initial displacement, the amplitudes of the successive cycles

were measured and plotted to a logarithmic scale against time. Inasmuch as the damping is of a logarithmic nature, the resulting plot is a straight line from which may be read the time for the motion to damp to one-half amplitude $\left(t_{1/2}\right)$.

For a system having a single degree of freedom in yaw such that for the stability-axis system the angle of sideslip β is the negative of the angle of yaw ψ, the equation of motion can be expressed as

$$\left(I_Z - N_{\dot{\psi}}\right)\ddot{\psi} - \left(N_{\dot{\psi}} - N_{\dot{\beta}} + N_{\dot{\psi}_f}\right)\dot{\psi} - \left(N_{\psi} - N_{\beta}\right)\psi = 0 \tag{1}$$

where $N_{\dot{\psi}_f}$ and N_{ψ} refer to the mechanical friction of the system and the flexure-pivot spring constant, respectively. The solution of equation (1) can be written as

$$\psi = e^{-mt}(A \sin 2\pi ft + B \cos 2\pi ft) \tag{2}$$

where

$$2\pi f = \sqrt{\frac{N_{\psi} - N_{\beta}}{I_Z - N_{\ddot{\psi}}} - \left[\frac{N_{\dot{\psi}} - N_{\dot{\beta}} + N_{\dot{\psi}_f}}{2\left(I_Z - N_{\ddot{\psi}}\right)}\right]^2}$$

$$m = -\frac{N_{\dot{\psi}} - N_{\dot{\beta}} + N_{\dot{\psi}_f}}{2\left(I_Z - N_{\ddot{\psi}}\right)}$$

The damping constant may be expressed in terms of the time to damp to one-half amplitude as

$$m = \frac{-0.693}{t_{1/2}}$$

The directional stability and damping of the system may then be expressed in nondimensional form in a manner similar to that of reference 5 as

$$C_{n_\beta} + C_{n_{\dot{r}}} k^2 \left(\frac{b_w}{c_t}\right)^2 = \frac{1}{qS_w b_w}\left[\left(I_Z - N_{\ddot{\psi}}\right)(2\pi f)^2 - N_{\psi}\right] \tag{3}$$

$$C_{n_r} - C_{n_{\dot{\beta}}} = \frac{-2.772\left(I_Z - N_{\ddot{\psi}}\right)V}{qS_w b_w^2}\left[\frac{1}{t_{1/2}} - \left(\frac{1}{t_{1/2}}\right)_{\text{wind off}}\right] \quad (4)$$

In order to find the damping due to friction in the system, the damping of the model is determined at zero wind velocity with an equivalent mass in place of the vertical tail and a torque rod of sufficient strength to produce the proper frequency inserted in the system. The term $N_{\ddot{\psi}}$ is interpreted in terms of a factor added to C_{n_β} because this particular group of free-damping tests afforded no convenient means for its separation. For the frequencies employed in these tests the factor $C_{n_{\dot{r}}} k^2 \left(\frac{b_w}{c_t}\right)^2$ should be small in comparison with C_{n_β}.

The damping derivatives were obtained from data similar to the sample records of model motion and plots of logarithm of amplitude against time given as figure 5. A small residual yawing motion of the model attributable to turbulence in the tunnel air stream necessitated determining the time to damp to one-half amplitude by the slope of the amplitude envelope at the largest angles of yaw in order to minimize the error in determining the damping derivatives. This source is believed to have resulted in no more than a 5-percent uncertainty in the results.

ANALYTICAL CONSIDERATIONS

Various unsteady-lift theories were employed to calculate the contributions of the vertical tail to the directional stability and damping of the model for comparison with the experimental results. These theories included the incompressible cases covered by Theodorsen for two dimensions and by Jones (reference 7), Reissner (reference 8), and Biot and Boehnlein (reference 9) with various degrees of approximation for finite span. The two-dimensional work including the subsonic effects of compressibility as given by Possio and Frazer and Skan is also employed. A short summary indicating procedures for obtaining the necessary derivatives from these theories is included here for completeness.

Two-Dimensional Derivatives

The work of Theodorsen on the derivation of the expressions for the unsteady lift and moment of a two-dimensional surface undergoing sinusoidal oscillations in an incompressible fluid is given in

reference 6. From this source, the moment per unit span about the airplane center of gravity of a vertical tail mounted on an airplane which is performing sideslipping oscillations can be shown to be

$$N(\beta) = -\pi q c_t^2 \left[\frac{a c_t \dot{\beta}}{4V} + \left(a + \frac{1}{2} \right) C(k) \beta \right] \tag{5}$$

A similar expression for an airplane performing yawing oscillations is

$$N(\psi) = -\frac{\pi}{2} q c_t^3 \left\{ \left[\frac{1}{4} - C(k) \left(\frac{1}{4} - a^2 \right) \right] \frac{\dot{\psi}}{V} + \frac{c_t}{4} \left(\frac{1}{8} + a^2 \right) \frac{\ddot{\psi}}{V^2} \right\} \tag{6}$$

An appendix to this paper gives a discussion of the conversion of these results from reference 6.

The Theodorsen function $C(k)$ is a complex circulation function of the reduced frequency and in terms of its real and imaginary parts is written

$$C(k) = F + iG$$

The functions F and G may be computed from expressions given in reference 6 in terms of Bessel functions of the first and second kinds of orders zero and one and of argument k. In stability practice equations (5) and (6) are usually interpreted in terms of derivatives as follows:

$$\left.\begin{aligned} N(\beta) &= C_{n_\beta} q S_w b_w \beta + C_{n_{\dot{\beta}}} \frac{q S_w b_w^2}{2V} \dot{\beta} \\ N(\psi) &= C_{n_r} \frac{q S_w b_w^2}{2V} \dot{\psi} + C_{n_{\dot{r}}} \frac{q S_w b_w^3}{4V^2} \ddot{\psi} \end{aligned}\right\} \tag{7}$$

If the sinusoidal motions

$$\beta = \beta_o e^{i\omega t}$$

$$\psi = \psi_o e^{i\omega t}$$

are employed for a substitution into equations (5), (6) and (7), the real and imaginary terms may be equated and the derivatives C_{n_β}, $C_{n_{\dot{\beta}}}$, C_{n_r}, and $C_{n_{\dot{r}}}$ determined. The results of such an analysis would be as follows:

$$\left.\begin{aligned} C_{n_\beta} &= -\frac{S_t}{S_w}\frac{c_t}{b_w}\pi\left(a + \frac{1}{2}\right)F \\ C_{n_{\dot{\beta}}} &= -\frac{S_t}{S_w}\left(\frac{c_t}{b_w}\right)^2\pi\left[\frac{a}{2} + \left(a + \frac{1}{2}\right)\frac{G}{k}\right] \\ C_{n_r} &= \frac{S_t}{S_w}\left(\frac{c_t}{b_w}\right)^2\pi\left[-\frac{1}{4} + F\left(\frac{1}{4} - a^2\right)\right] \\ C_{n_{\dot{r}}} &= \frac{S_t}{S_w}\left(\frac{c_t}{b_w}\right)^3\pi\left[\frac{1}{2}\left(\frac{1}{8} + a^2\right) + \frac{G}{k}\left(\frac{1}{4} - a^2\right)\right] \end{aligned}\right\} \quad (8)$$

The velocity terms contain only the F term of the Theodorsen function whereas the acceleration terms contain the G term divided by k. The corresponding side-force derivatives are derived in the appendix. For the free-oscillation tests conducted for this paper, the motion is such that the angle of sideslip is the negative of the angle of yaw. The damping derivative measured therefore is the difference between the derivatives C_{n_r} and $C_{n_{\dot{\beta}}}$ determined from equation (8). This fact was illustrated previously with respect to the reduction of the oscillation test data. In a like manner, the directional stability parameter measured can be shown to be a combination of the C_{n_β} and $C_{n_{\dot{r}}}$ terms, specifically

$$C_{n_\beta} + C_{n_{\dot{r}}}k^2\left(\frac{b_w}{c_t}\right)^2$$

Combination of the results of equations (8) to obtain the factors calculated for comparison with the oscillation tests gives

$$\left.\begin{aligned} C_{n_r} - C_{n_{\dot{\beta}}} &= -\frac{\pi}{2}\left(\frac{c_t}{b_w}\right)^2 \frac{S_t}{S_w}\frac{B}{k} \\ C_{n_\beta} + C_{n_r} k^2\left(\frac{b_w}{c_t}\right)^2 &= -\frac{\pi}{2}\frac{c_t}{b_w}\frac{S_t}{S_w} A \end{aligned}\right\} \tag{9}$$

where

$$B = -\left(a - \frac{1}{2}\right)k - \left(a + \frac{1}{2}\right)2G + \left(a^2 - \frac{1}{4}\right)2kF$$

$$A = \left(a^2 + \frac{1}{8}\right)k^2 + \left(a + \frac{1}{2}\right)2F + \left(a^2 - \frac{1}{4}\right)2kG$$

Finite-Span Derivatives

The aerodynamic-span effect is considered in reference 7 for wings of aspect ratios of 6 and 3 by correcting the aerodynamic inertia and the angle of attack of the infinite-span surface. An approximation employed in this analysis concerning motions of long wave length may make the results subject to question for values of k near zero. The reference presents expressions for calculating the finite-span values of the Theodorsen function $C(k)$. The use of these F and G circulation functions in equations (8) and (9) results in values of the various derivatives considered for aspect ratios of 6 and 3.

The aerodynamic-span effect is considered for wings of arbitrary aspect ratio in reference 8. The three-dimensional effect of the finite span may be obtained by adding a correction term σ to the basic Theodorsen two-dimensional function. The finite-span function $C(k) + \sigma$ is employed in a rather lengthy and tedious computation in order to determine the components of the unsteady lift for each of five points along the span of the oscillating surface. The various stability derivatives may then be determined by a graphical integration of the in-phase and out-of-phase components. An approximation made in this analysis is of such a nature as to make the method primarily suited to the higher aspect ratios. A practical lower limit of applicability is not known.

A one-point approximation to the span effect for the calculation of the unsteady lift may be employed rather than the five-point procedure. Comparative calculations made for the present investigation

have shown the one-point approximation to yield results for low aspect ratios which are essentially the same as those calculated by the longer procedure.

Biot and Boehnlein (reference 9) considered the aerodynamic-span effect on unsteady lift by an approach that yields a closed form for a one-point approximation to the span effect. The finite-span circulation functions used are

$$\overline{P} = F + iG$$

$$\overline{Q} = H + iJ$$

For infinite aspect ratio

$$\overline{P} = \overline{Q} = C(k)$$

where $C(k)$ is the two-dimensional Theodorsen function. The functions $\overline{P}$ and $\overline{Q}$ may be calculated for the argument k by methods given in reference 9, and equations (8) and (9) are again used to calculate the various stability derivatives. The factors A and B which appear in equations (9) must, however, be written in terms of $\overline{P}$ and $\overline{Q}$ as follows:

$$A = (2a - 1)akG + \left(a - \frac{1}{2}\right)kJ + \left(a^2 + \frac{1}{8}\right)k^2 + 2aF + H$$

$$B = (2a - 1)akF + \left(a - \frac{1}{2}\right)kH - \left(a - \frac{1}{2}\right)k - 2aG - J$$

Effect of Compressibility

Subsonic compressibility effects on the unsteady damping in yaw and directional stability of a two-dimensional oscillating lifting surface can be considered through the use of reference 10 which is an extension of the calculations of Possio (reference 11). The infinite-span compressible-flow values for the stability derivatives can be obtained by the use of equations (8) and (9) for Mach numbers 0, 0.5, and 0.7. In the notation of Frazer and Skan (reference 10), however,

$$A = 4M_3 - \frac{1}{2}\left(\frac{1}{2} + a\right)\left(M_1 + Z_3 - \frac{a}{2}Z_1\right) + M_1$$

$$B = 4M_4 - \frac{1}{2}\left(\frac{1}{2} + a\right)\left(M_2 + Z_4 - \frac{a}{2}Z_2\right) + M_2$$

The correspondence between the notation of Theodorsen and that of Frazer and Skan is shown in reference 12. The values of the Z and M functions are tabulated by Frazer and Skan for Mach numbers 0, 0.5, and 0.7 and a significant range of reduced frequencies. Reissner has recently extended his work on oscillating wings of finite span to include, to the same degree of approximation as for the incompressible case, the subsonic effects of compressibility. (See reference 13.)

RESULTS AND DISCUSSION

Presentation of Results

The experimental values of the longitudinal, directional, and yawing characteristics of the complete model, the model with wing removed and the fuselage alone as determined by force tests are given in figure 6. The experimental values of the damping in yaw of the fuselage and tail assembly (designated FT) and the fuselage alone (designated F) obtained by the freely damped oscillation technique for several frequencies of oscillation are shown in figures 7 and 8. The frequency and aspect-ratio effects on the damping in yaw contributed by the vertical tail as calculated from the unsteady-lift theories discussed previously are also shown in these figures. Figure 9 gives a comparison of the relative importance of C_{n_r} and $C_{n_{\dot{\beta}}}$ on the damping in yaw of the model. Figures 10 to 12 are similar figures summarizing frequency and aspect-ratio effects on directional stability. Figures 13 and 14 give the computed effects of compressibility on the vertical-tail contribution to the damping in yaw and directional stability of the test model.

Discussion

The variation of the experimentally determined damping in yaw of the test model with frequency is in reasonably good agreement for the range covered by the tests with the various approximate theoretical treatments which consider the effect of finite span. (See figs. 7 and 8.) The contribution of the fuselage to the damping in yaw is small for the range of test frequencies. A two-dimensional approximation to the damping as is frequently employed for flutter work appears to be remarkably good for $k > 0.1$ and for aspect ratios of 6 and greater (fig. 8). A large effect of aspect ratio, however, is shown for aspect ratios below 6 for the entire frequency range and for all aspect ratios for frequencies less than $k = 0.1$. The two-dimensional result indicates a loss in damping at low frequencies much greater than the finite-span result and, in fact, shows a reversal in sign of the damping at

sufficiently low frequencies. A number of papers dealing with unsteady lift have noted this characteristic of the two-dimensional aerodynamic forces. (See references 1 to 3 and 14.)

An examination of the values of the derivatives C_{n_r} and $C_{n_{\dot{\beta}}}$ as computed from reference 6 for infinite aspect ratio and reference 7 for aspect ratios of 3 and 6 (fig. 9) indicates that the derivative $C_{n_{\dot{\beta}}}$ is critically dependent on reduced frequency for the low range of reduced frequencies and infinite aspect ratio. The derivative C_{n_r} is only slightly dependent on the reduced frequency for infinite aspect ratio and even less so for the lower aspect ratios. The dependence of $C_{n_{\dot{\beta}}}$ on reduced frequency is responsible for the decrease in damping shown for the infinite-aspect-ratio case as the frequency is reduced (figs. 7 and 8).

The aspect-ratio-2 results shown in figures 7 and 10 were obtained from the theory of Jones (reference 7) for aspect ratio 3 by use of a correction factor which was the ratio of the lifting-line-theory lift-curve slopes for aspect ratios of 2 and 3. This correction is only approximate and was made in order to place the results on a comparable basis. The variation of $C_{n_r} - C_{n_{\dot{\beta}}}$ with reduced frequency, shown in figure 7, indicates no appreciable effect of frequency to zero frequency. In fact, the result of Jones for aspect ratio 3 reduces to a finite value at $k = 0$ given by

$$C_{n_r} - C_{n_{\dot{\beta}}} = -\frac{\pi}{2}\left(\frac{c_t}{b_w}\right)^2 \frac{S_t}{S_w}\left(1.2a^2 - 0.370a + 0.515\right)$$

which is not the case for the two-dimensional result that approaches infinity as k approaches zero. This result is not expected to be very accurate close to $k = 0$, however, because of the nature of the assumptions made in its derivation as mentioned previously.

When the finite-span effects are considered, it appears that these effects are especially significant with regard to the damping in yaw of this model for aspect ratios smaller than 6. (See fig. 8.) The theory also indicates a significant decrease in the damping at low frequencies when the aspect ratio was increased from 20 to ∞.

The experimental values of damping in yaw obtained by free oscillation agree closely with the values of C_{n_r} obtained by the standard curved-flow testing procedure used in the Langley stability tunnel. The curved-flow technique results in the $k = 0$ value of C_{n_r}. No unsteady effects, however, are obtained by this technique.

The unsteady-lift theories indicate that, at frequencies of oscillation from $k = 0$ to $k = 0.1$, the frequency has little effect on the directional stability contributed by the vertical tail but that high frequencies of oscillation can cause the directional stability contributed by the vertical tail to decrease greatly and eventually to change sign (figs. 10 and 11). Changes in aspect ratio, for low aspect ratios, have a large effect on the directional stability; for high aspect ratios, changes in aspect ratio are less significant. The experimental values of directional stability obtained from the free-damping tests remained constant for the range of frequencies investigated, although the magnitudes are somewhat smaller than those predicted for the tail contribution by the calculation methods for aspect ratio 2. This result is not unexpected because all the finite-span unsteady-lift theories employed maintain some resemblance to the Prandtl lifting-line theory which, of course, yields values of the lift-curve slope for low aspect ratios which are unrealistically high. The values of directional stability obtained by both the free-oscillation and curved-flow procedures were about the same magnitude.

Figure 12 gives a comparison of the contribution of a vertical tail to the stability derivatives C_{n_β} and $C_{n_{\dot{r}}}$ as computed from references 6 and 7. These derivatives were combined in the proportion

$$C_{n_\beta} + C_{n_{\dot{r}}} k^2 \left(\frac{b_w}{c_t}\right)^2$$

for comparison with the results of the oscillation tests. Although $C_{n_{\dot{r}}}$ is of appreciable magnitude itself, the factor $C_{n_{\dot{r}}} k^2 \left(\frac{b_w}{c_t}\right)^2$ is very small relative to C_{n_β} for the range of frequencies around $k = 0.01$ and thus should not greatly affect the directional stability of the usual airplane.

The computed two-dimensional Mach number effects on the damping in yaw and directional stability of the tail surface of the test model are shown in figures 13 and 14. These results were included to illustrate the powerful effect of compressibility on the damping contributed by the tail surface. A complete coverage of one-degree-of-freedom flutter by use of these aerodynamic forces which may be obtained from references 10 to 12 is given in reference 14. Compressibility effects decrease the tail-surface damping at low frequencies and increase the damping at higher frequencies. The directional stability increases at all frequencies with increase in Mach number with the largest increases occurring in the high-frequency range of oscillations. Reference 15 which presents the two-dimensional oscillating aerodynamic forces at

sonic speed indicates larger deviations from the results for incompressible flow than for the subsonic results given here.

CONCLUSIONS

The following conclusions were drawn from the results of an investigation made at a Mach number of 0.14 of the effects of frequency and aspect ratio on the directional damping and stability of a fuselage and vertical tail oscillating freely in yaw:

1. The contribution of the vertical tail to the damping in yaw of the model agreed within the limits of experimental accuracy with predictions of the approximate finite-aspect-ratio unsteady-lift theories for the range of frequencies tested.

2. Two-dimensional unsteady-lift theory predicted a much greater loss in damping with reduction in frequency than was shown by experiment or by the approximate finite-aspect-ratio unsteady-lift theories.

3. Both the unsteady-lift theories and the experimental results indicated that the contribution of the vertical tail to the directional stability of the model was relatively independent of frequency for frequencies comparable to those of lateral airplane motions.

Langley Aeronautical Laboratory
National Advisory Committee for Aeronautics
Langley Field, Va., November 26, 1951

APPENDIX

CONVERSION OF UNSTEADY FORCES AND MOMENTS FROM FLUTTER TO STABILITY AXES

The conversion of the contribution of the vertical tail to the yawing moment of an airplane in terms of unsteady-lift functions and the Theodorsen flutter axes to the stability axes which are fixed in the body is included here as a matter of general interest. Reference 16 gives considerable attention to such axis conversions. The following sketches indicate the paths and attitudes of airplanes performing sinusoidal sideslipping and yawing oscillations within the limits of the stability-axis system:

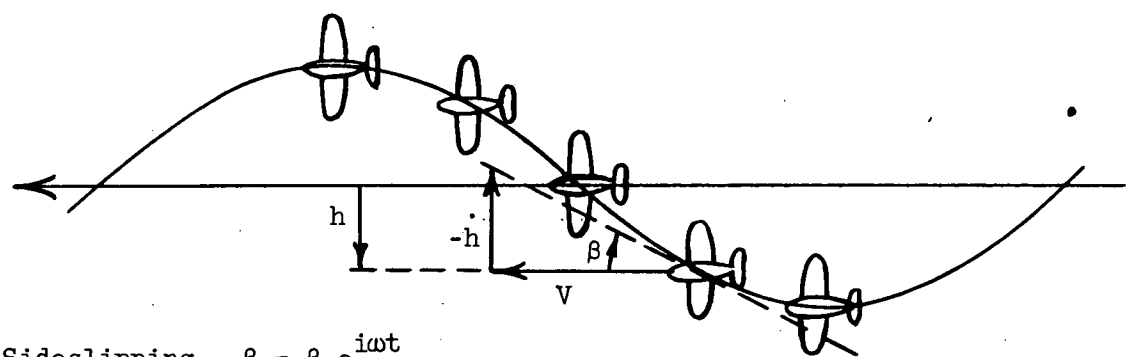

Sideslipping, $\beta = \beta_o e^{i\omega t}$

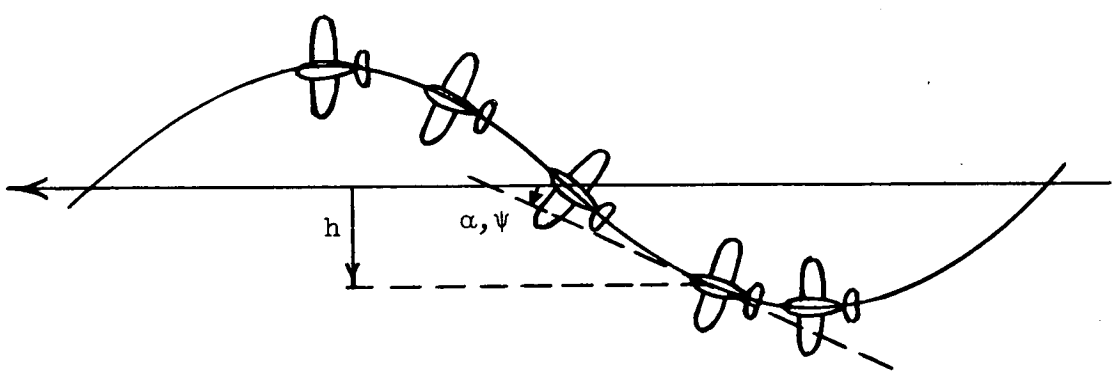

Yawing, $\psi = \psi_o e^{i\omega t}$

The Theodorsen coordinates h and α and the stability-axis coordinates β and ψ are shown with respect to the paths followed by the airplanes in sideslipping and yawing flight.

In sideslipping flight

$$\beta = -\frac{1}{V}\dot{h}$$

$$\alpha = 0$$

and in yawing flight

$$\psi = -\frac{1}{V}\dot{h} = \alpha$$

From reference 6 the contribution of the vertical tail to the yawing moment of an airplane in terms of the flutter coordinates is

$$N(\alpha,h) = -\frac{\rho c_t^2}{4}\left[\pi\left(\frac{1}{2} - a\right)\frac{Vc_t}{2}\dot{\alpha} + \frac{\pi c_t^2}{4}\left(\frac{1}{8} + a^2\right)\ddot{\alpha} - \frac{a\pi c_t}{2}\ddot{h}\right] + \rho V \frac{c_t^2}{2}\pi\left(a + \frac{1}{2}\right)C(k)\left[V\alpha + \dot{h} + \frac{c_t}{2}\left(\frac{1}{2} - a\right)\dot{\alpha}\right]$$

If this moment is for a sideslipping motion or a yawing motion in the sense given by stability axes fixed in the body and the following terms are substituted for the sideslipping case

$$\alpha = 0$$

$$\dot{\alpha} = 0$$

$$\ddot{\alpha} = 0$$

$$\dot{h} = -V\beta$$

$$\ddot{h} = -V\dot{\beta}$$

and for the yawing case

$$\dot{h} = -V\psi$$

$$\ddot{h} = -V\dot{\psi}$$

$$\alpha = \psi$$

$$\dot{\alpha} = \dot{\psi}$$

$$\ddot{\alpha} = \ddot{\psi}$$

the following results are obtained for the sideslipping case

$$N(\beta) = -\frac{\rho c_t^2}{4}\left(\frac{a\pi c_t V}{2}\dot{\beta}\right) + \frac{\rho V c_t^2 \pi}{2}\left(a + \frac{1}{2}\right)C(k)(-V\beta)$$

and for the yawing case

$$N(\psi) = -\frac{\rho c_t^2}{4}\left[\pi\left(\frac{1}{2} - a\right)\frac{Vc_t}{2}\dot{\psi} + \frac{\pi c_t^2}{4}\left(\frac{1}{8} + a^2\right)\ddot{\psi} + \frac{a\pi c_t V}{2}\dot{\psi}\right] +$$

$$\frac{\rho V c_t^2}{2}\pi\left(a + \frac{1}{2}\right)C(k)\left[\frac{c_t}{2}\left(\frac{1}{2} - a\right)\dot{\psi}\right]$$

which reduce for the sideslipping case to

$$N(\beta) = -\pi q c_t^2\left[\frac{a c_t \dot{\beta}}{4V} + \left(a + \frac{1}{2}\right)C(k)\beta\right]$$

and for the yawing case to

$$N(\psi) = -\frac{\pi}{2} q c_t^3\left\{\left[\frac{1}{4} - C(k)\left(\frac{1}{4} - a^2\right)\right]\frac{\dot{\psi}}{V} + \frac{c_t}{4}\left(\frac{1}{8} + a^2\right)\frac{\ddot{\psi}}{V^2}\right\}$$

Similar expressions may be obtained for the side force in pure sideslipping and yawing flight. Reference 6 gives the side force of the

vertical tail in terms of the flutter axes as

$$Y(\alpha,h) = -\frac{\rho c_t^2}{4}\left(V\pi\dot{\alpha} + \pi\ddot{h} - \frac{\pi c_t a\ddot{\alpha}}{2}\right) - \pi\rho V c_t C(k)\left[V\alpha + \dot{h} + \frac{c_t}{2}\left(\frac{1}{2} - a\right)\dot{\alpha}\right]$$

which, when the following terms are substituted for the sideslipping case

$$\dot{h} = -V\beta$$

$$\ddot{h} = -V\dot{\beta}$$

$$\alpha = 0$$

$$\dot{\alpha} = 0$$

$$\ddot{\alpha} = 0$$

and for the yawing case

$$\dot{h} = -V\psi$$

$$\ddot{h} = -V\dot{\psi}$$

$$\alpha = \psi$$

$$\dot{\alpha} = \dot{\psi}$$

$$\ddot{\alpha} = \ddot{\psi}$$

becomes for pure sideslipping and yawing flight

$$Y(\beta) = qc_t\frac{\pi}{2}\left[c_t\left(\frac{\dot{\beta}}{V}\right) + 4C(k)\beta\right]$$

and

$$Y(\psi) = -qc_t^2\frac{\pi}{2}\left[C(k)\left(\frac{1}{2} - a\right)\frac{\dot{\psi}}{V} - \frac{c_t}{2}a\frac{\ddot{\psi}}{V^2}\right]$$

Substituting the motions, in the manner done in the text, for the yawing moment,

$$\beta = \beta_o e^{i\omega t}$$

$$\psi = \psi_o e^{i\omega t}$$

into these expressions and into the expressions in terms of stability derivatives which are

$$Y(\beta) = C_{Y_\beta} \beta q S_w + C_{Y_{\dot{\beta}}} \dot{\beta} \frac{q S_w b_w}{2V}$$

$$Y(\psi) = C_{Y_{\dot{r}}} \dot{\psi} \frac{q S_w b_w}{2V} + C_{Y_{\ddot{r}}} \ddot{\psi} \frac{q S_w b_w^2}{4V^2}$$

gives the following relationships for the tail contribution to the side-force derivatives when the real and imaginary parts of these equations are equated:

Page 22: Last four equations should be:

$$C_{Y_\beta} = -2\pi \frac{S_t}{S_w} F$$

$$C_{Y_{\dot{\beta}}} = -\pi \frac{S_t}{S_w} \frac{c_t}{b_w} \left(1 + 2 \frac{G}{k}\right)$$

$$C_{Y_{\dot{r}}} = 2 \frac{S_t}{S_w} \frac{c_t}{b_w} \pi F \left(\frac{1}{2} - a\right)$$

$$C_{Y_{\ddot{r}}} = - \frac{S_t}{S_w} \left(\frac{c_t}{b_w}\right)^2 \pi \left[a - 2 \frac{G}{k} \left(\frac{1}{2} - a\right)\right]$$

REFERENCES

1. Glauert, H.: The Force and Moment on an Oscillating Aerofoil. R. & M. No. 1242, British A.R.C., 1929.

2. Smilg, Benjamin: The Instability of Pitching Oscillations of an Airfoil in Subsonic Incompressible Potential Flow. Jour. Aero. Sci., vol. 16, no. 11, Nov. 1949, pp. 691-696.

3. Goland, Martin: The Quasi-Steady Air Forces for Use in Low-Frequency Stability Calculations. Jour. Aero. Sci., vol. 17, no. 10, Oct. 1950, pp. 601-608.

4. Runyan, Harry L., and Watkins, Charles E.: Considerations on the Effect of Wind-Tunnel Walls on Oscillating Air Forces for Two-Dimensional Subsonic Compressible Flow. NACA TN 2552, 1951.

5. Campbell, John P., and Mathews, Ward O.: Experimental Determination of the Yawing Moment Due to Yawing Contributed by the Wing, Fuselage, and Vertical Tail of a Midwing Airplane Model. NACA ARR 3F28, 1943.

6. Theodorsen, Theodore: General Theory of Aerodynamic Instability and the Mechanism of Flutter. NACA Rep. 496, 1935.

7. Jones, Robert T.: The Unsteady Lift of a Wing of Finite Aspect Ratio. NACA Rep. 681, 1940.

8. Reissner, Eric, and Stevens, John E.: Effect of Finite Span on the Airload Distributions for Oscillating Wings. II - Methods of Calculation and Examples of Application. NACA TN 1195, 1947.

9. Biot, M. A., and Boehnlein, C. T.: Aerodynamic Theory of the Oscillating Wing of Finite Span. GALCIT Rep. No. 5, Sept. 1942.

10. Frazer, R. A., and Skan, Sylvia W.: Influence of Compressibility on the Flexural-Torsional Flutter of Tapered Cantilever Wings. Rep. No. 5916, British A.R.C., June 30, 1942. (Reissued as R. & M. No. 2553.)

11. Possio, Camillo: L'Azione aerodinamica sul profilo oscillante in un fluido compressibile a velocita iposonora. L'Aerotecnica, vol. XVIII, fasc. 4, April 1938, pp. 441-458. (Available as British Air Ministry Translation No. 830.)

12. Garrick, I. E.: Bending-Torsion Flutter Calculations Modified by Subsonic Compressibility Corrections. NACA Rep. 836, 1946. (Supersedes NACA TN 1034.)

13. Reissner, Eric: Extension of the Theory of Oscillating Airfoils of Finite Span in Subsonic Compressible Flow. NACA TN 2274, 1951.

14. Runyan, Harry L.: Single-Degree-of-Freedom-Flutter Calculations for a Wing in Subsonic Potential Flow and Comparison with an Experiment. NACA TN 2396, 1951.

15. Nelson, Herbert C., and Berman, Julian H.: Calculations on the Forces and Moments for an Oscillating Wing-Aileron Combination in Two-Dimensional Potential Flow at Sonic Speed. NACA TN 2590, 1952.

16. Ashley, Holt: Some Unsteady Aerodynamic Problems Affecting the Dynamic Stability of Aircraft. M.I.T. Thesis, 1951.

TABLE I

EXPERIMENTAL RESULTS

Configuration	P (sec)		k	$t_{1/2}$ (sec)		I_Z (ft-lb-sec^2)	$-(C_{n_r} - C_{n_{\dot{\beta}}})$			$C_{n_\beta} + C_{n_r} k^2 \left(\frac{b_w}{c_t}\right)^2$
	Wind off	Wind on		Wind off	Wind on		Total	Friction	Aerodynamic	
Fuselage and tail	13.21	7.15	0.0012	190.08	85.80	32.89	0.610	0.275	0.335	0.204
	4.08	2.19	.0040	49.70	11.47	3.09	.429	.099	.330	.204
	3.96	2.25	.0039	54.65	10.35	3.09	.475	.090	.385	.190
	3.96	2.19	.0040	54.65	11.39	3.09	.432	.090	.342	.204
	.75	.77	.0114	34.36	1.72	.38	.351	.018	.333	.213
	.22	.30	.0293	3.40	.28	.06	.340	.028	.312	.203
Fuselage alone	.29	.27	.0321	13.80	3.21	.06	.030	.007	.023	-.058
	.75	.74	.0119	34.36	13.77	.38	.044	.018	.026	-.015

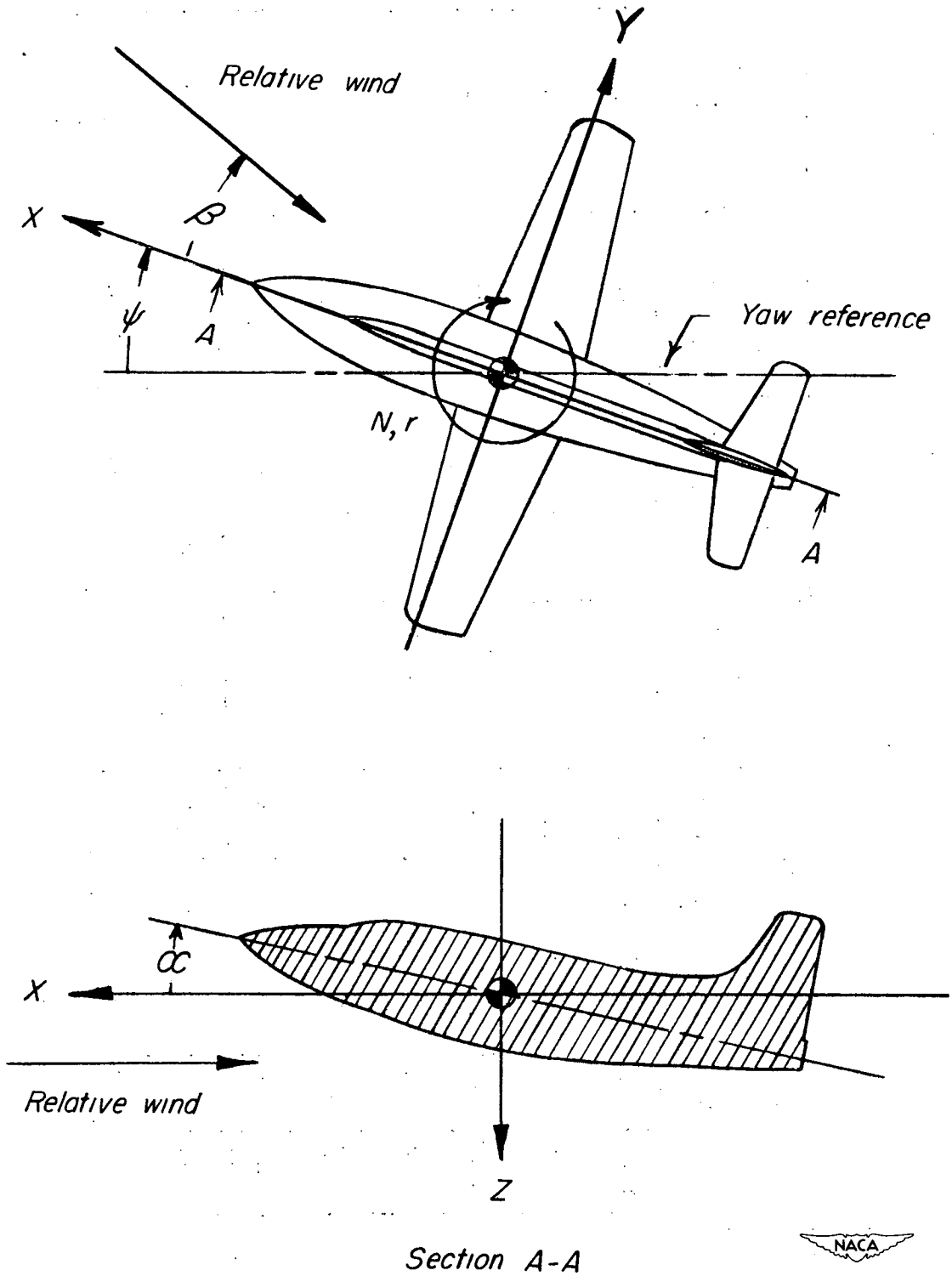

Figure 1.- System of stability axes. Arrows indicate positive forces, moments, and angular displacements. Yaw reference generally chosen to coincide with initial relative wind.

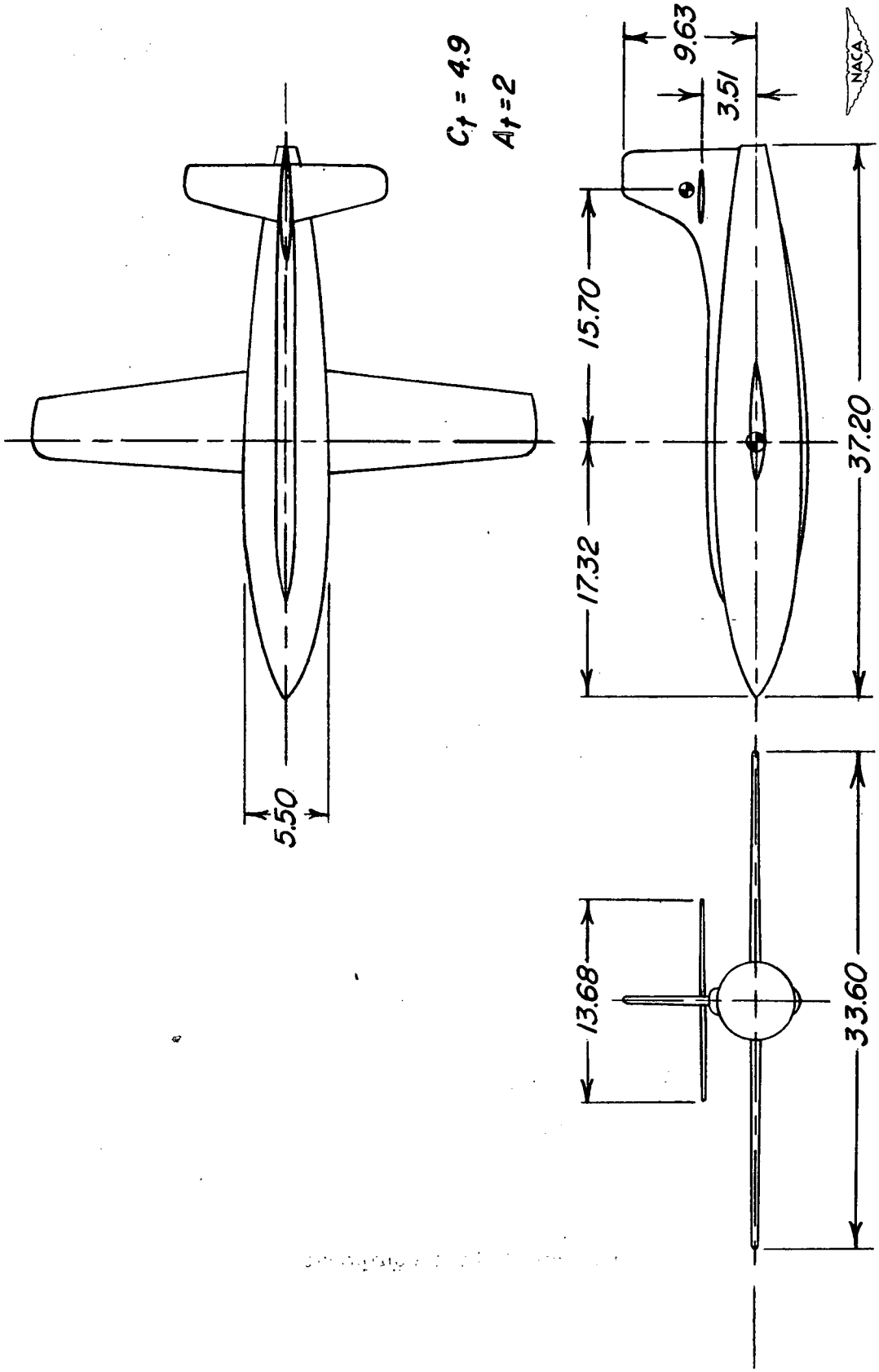

Figure 2.- Drawing of model tested. All dimensions are in inches.

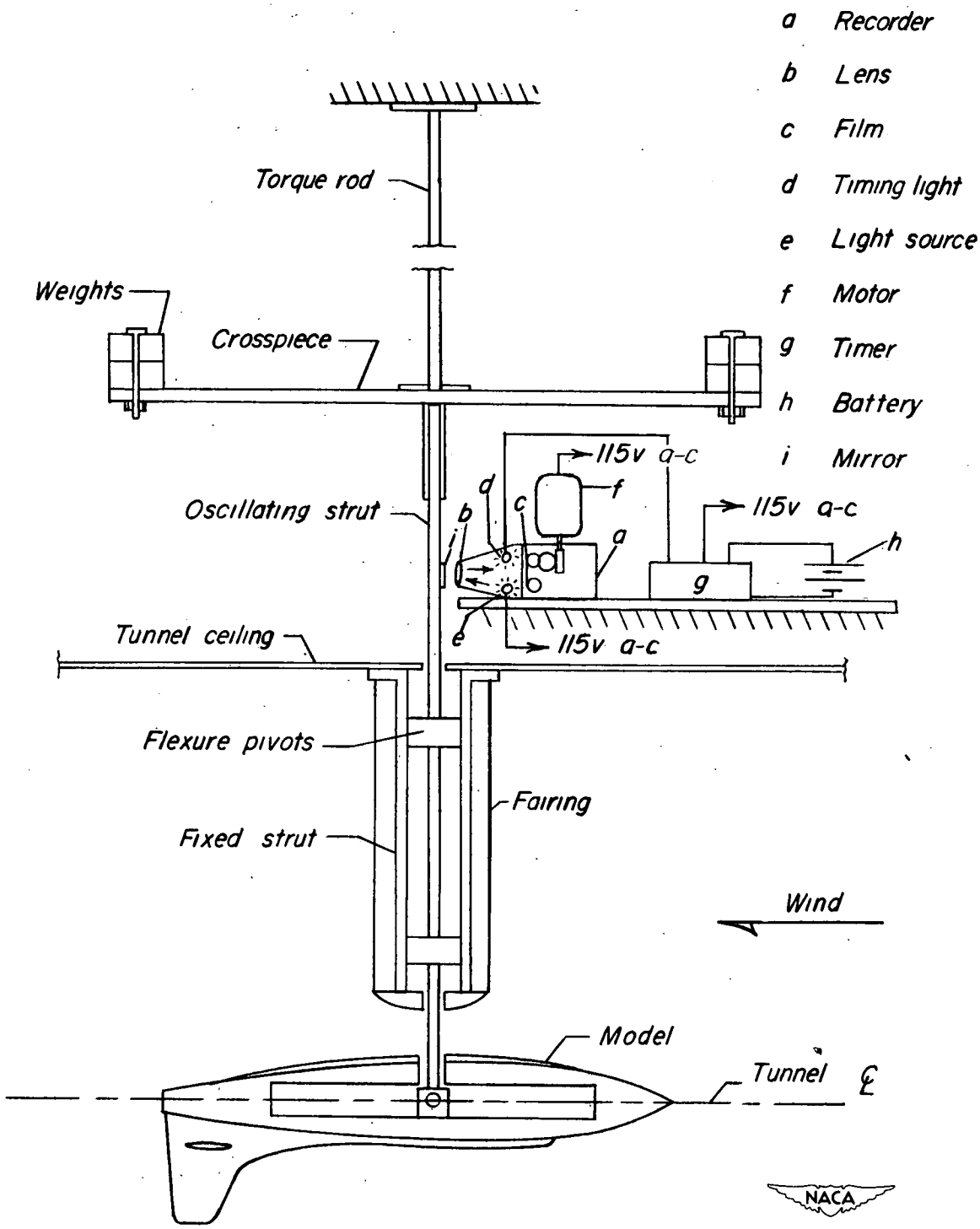

Figure 3.- Diagram of test equipment.

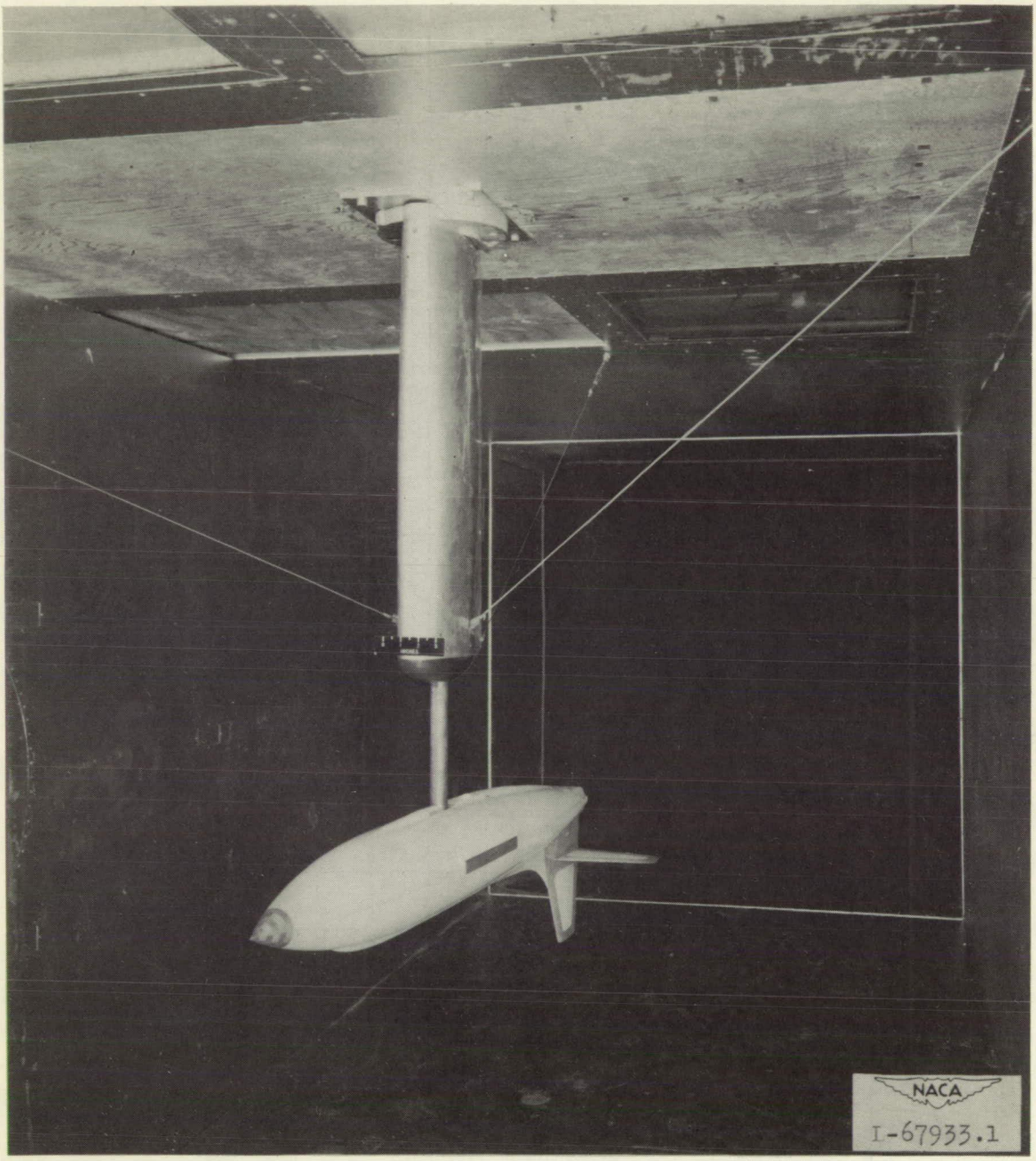

Figure 4.- Test model mounted on free-oscillation strut in Langley stability tunnel.

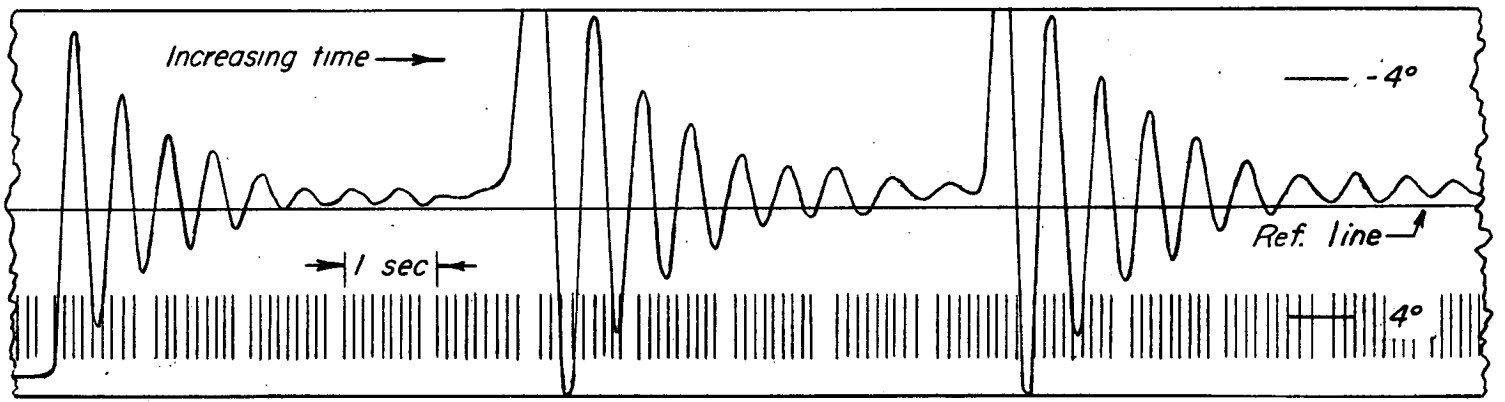

(a) Film record of yawing oscillation.

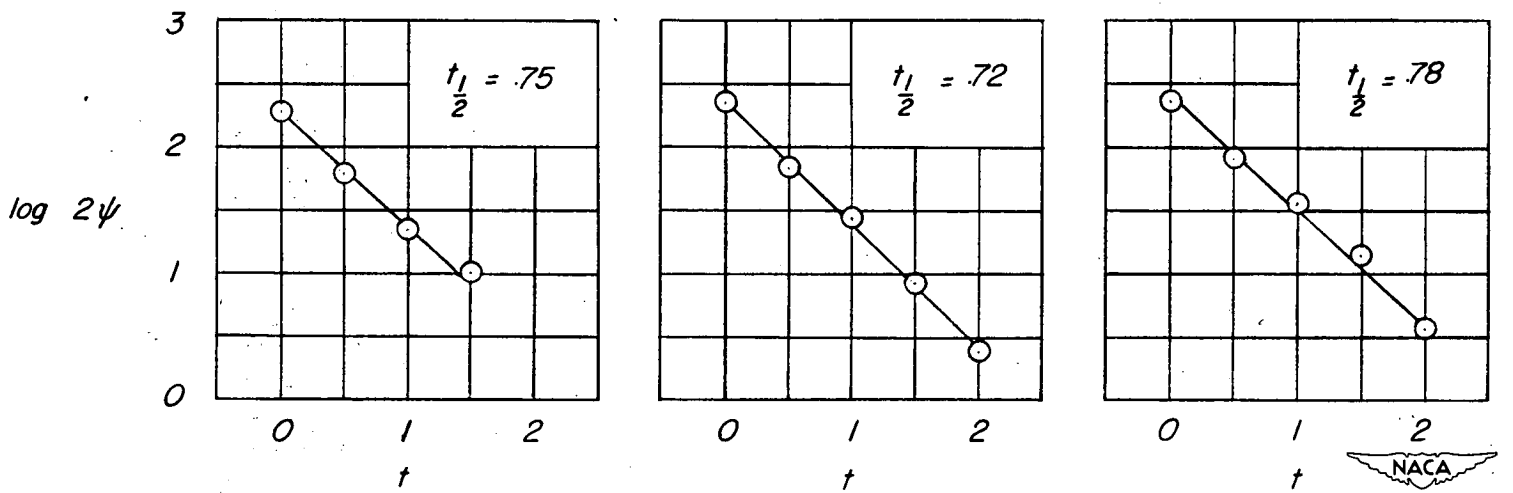

(b) Logarithmic plots of amplitude variation with time.

Figure 5.- Representative film record and resulting logarithmic plots.

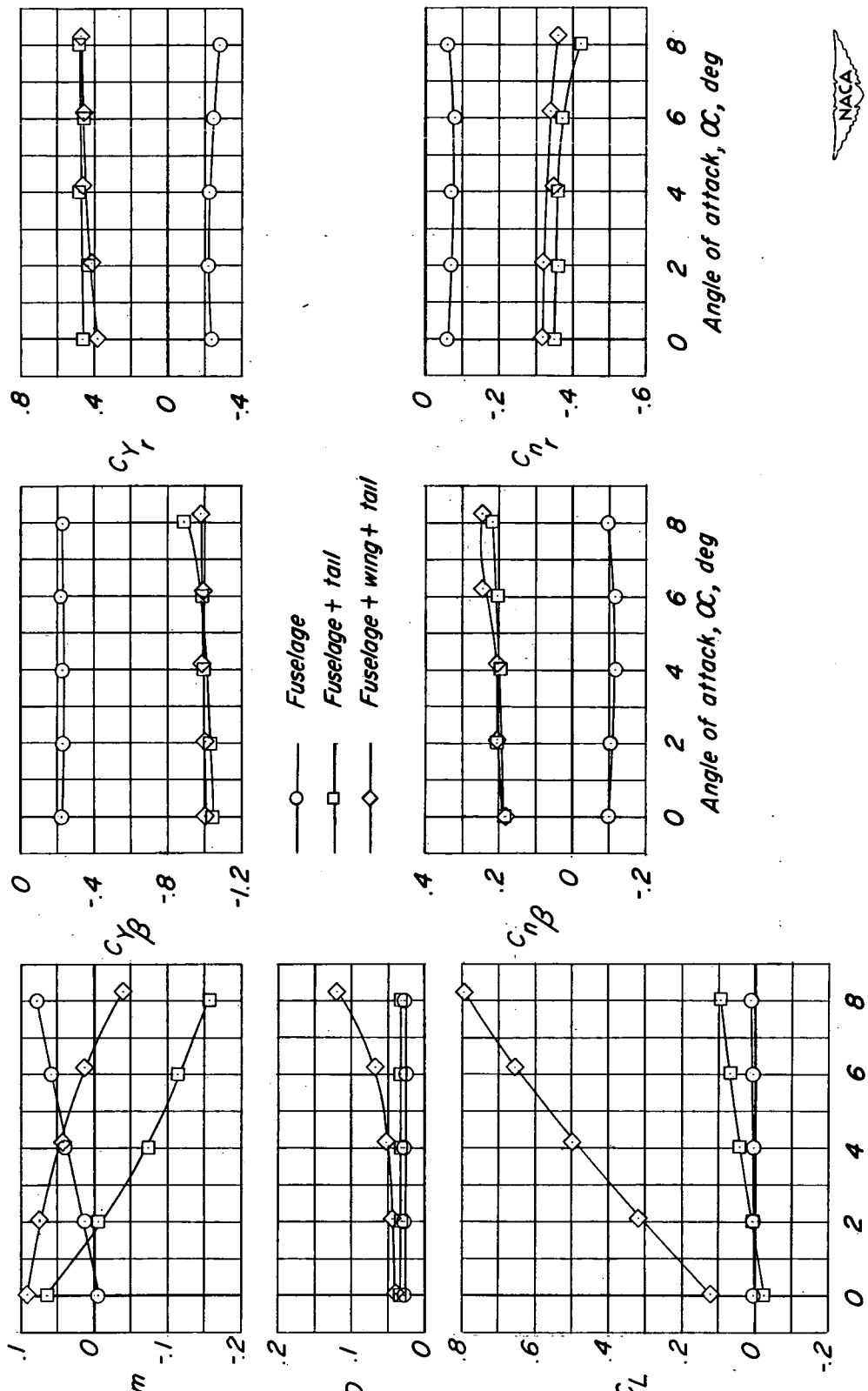

Figure 6.- The steady-state stability characteristics of the model tested.

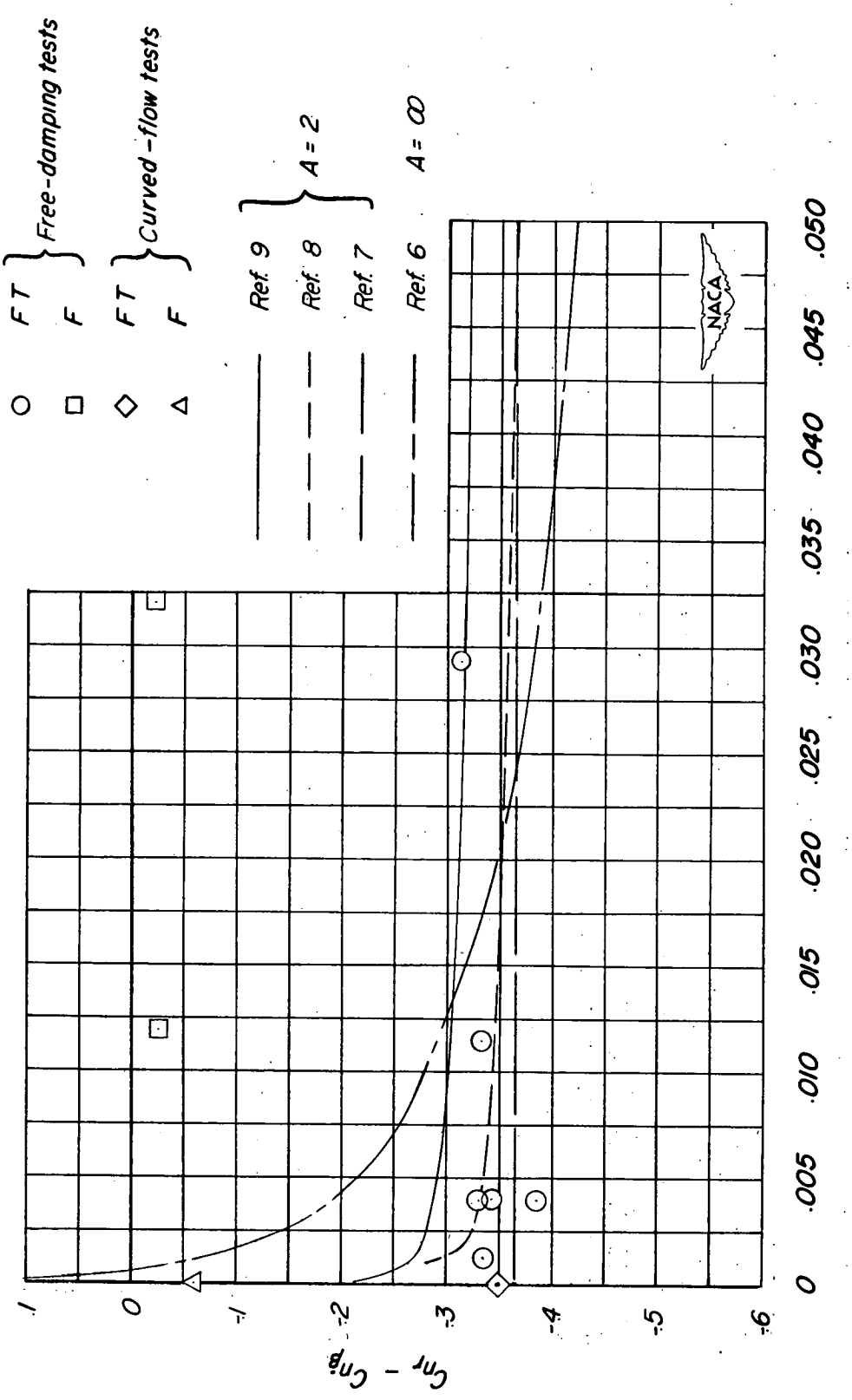

Figure 7.- The effect of frequency on the damping in yaw for a low range of the reduced frequency. Comparison of several methods for calculating frequency effect on C_{n_r}.

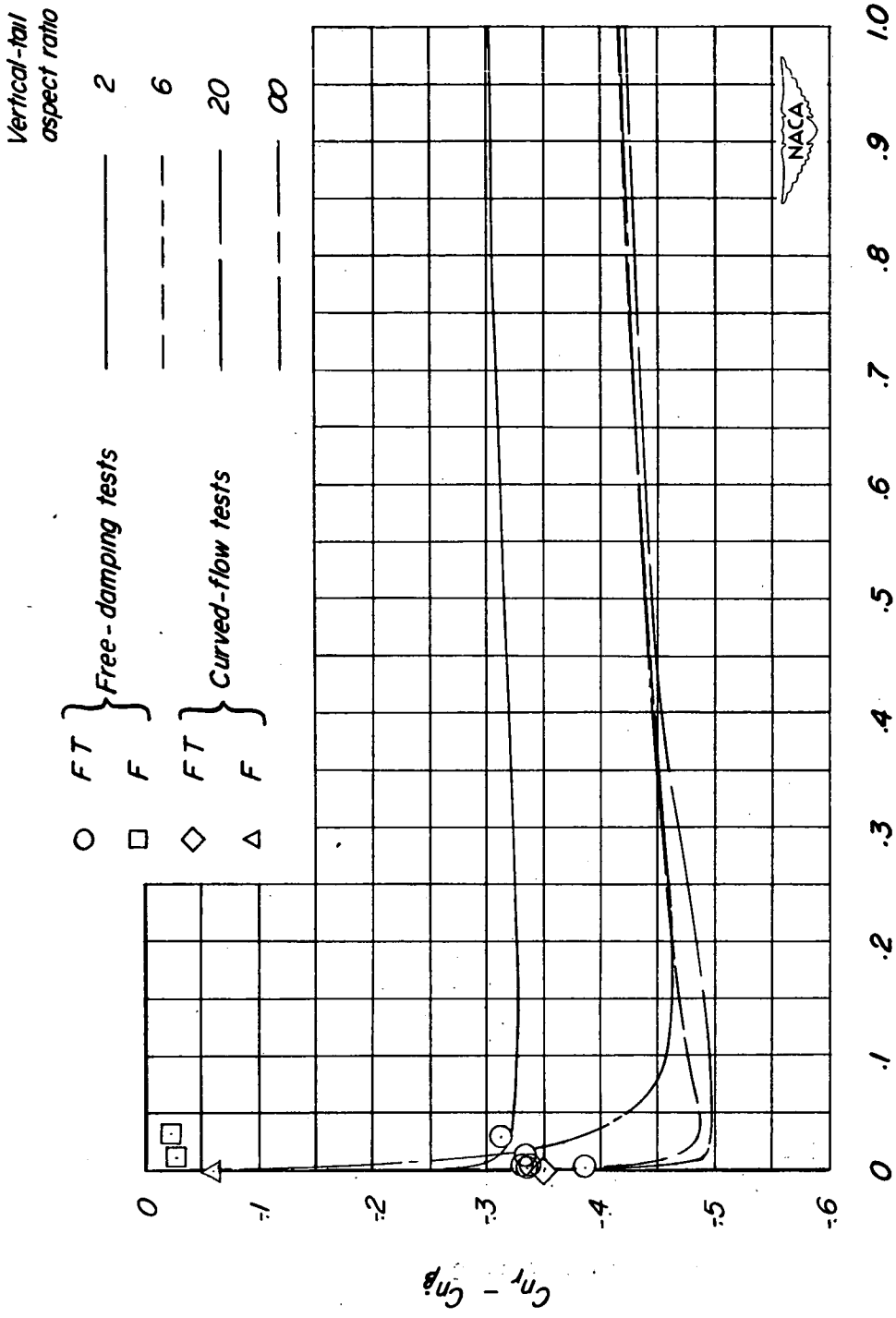

Figure 8.- The effect of aspect ratio on C_{n_r} as calculated by the method of Biot for a range of reduced frequencies.

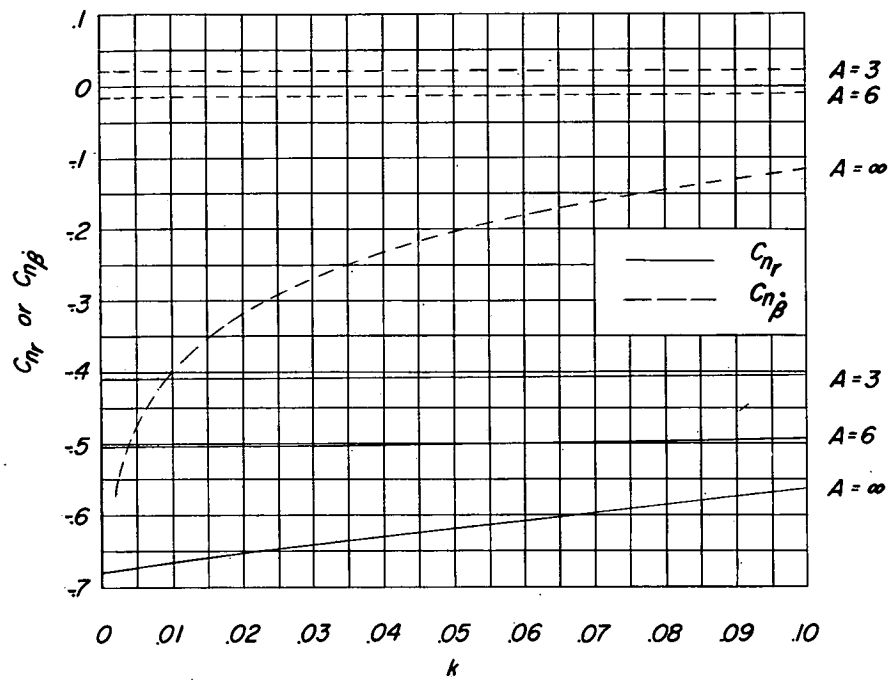

(a) Lower range of reduced frequencies.

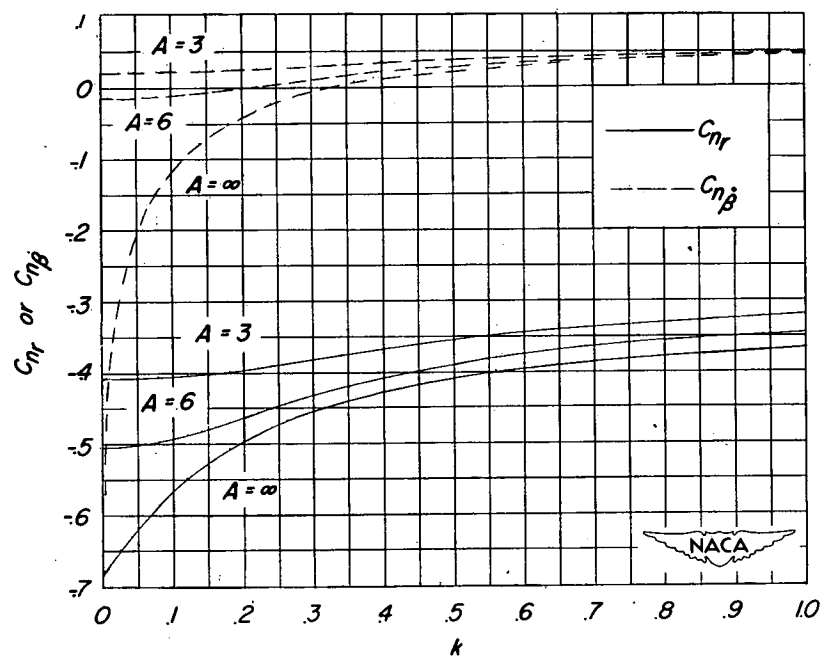

(b) Range of reduced frequencies.

Figure 9.- The effect of reduced frequency on the stability derivatives C_{n_r} and $C_{n_{\dot{\beta}}}$.

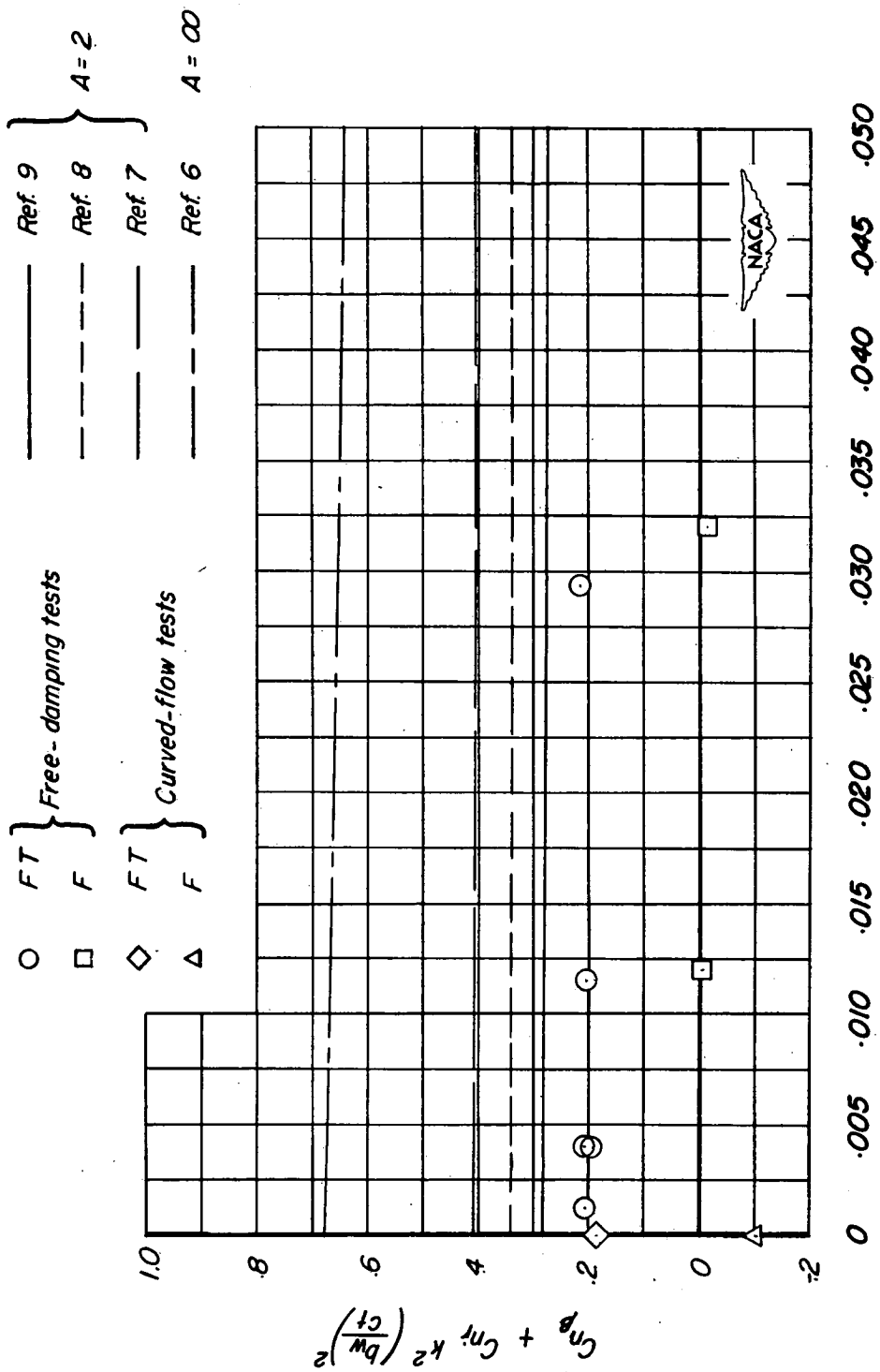

Figure 10.- The effect of frequency on the directional stability for a low range of the reduced frequency. Comparison of several methods for calculating frequency effect on C_{n_β}.

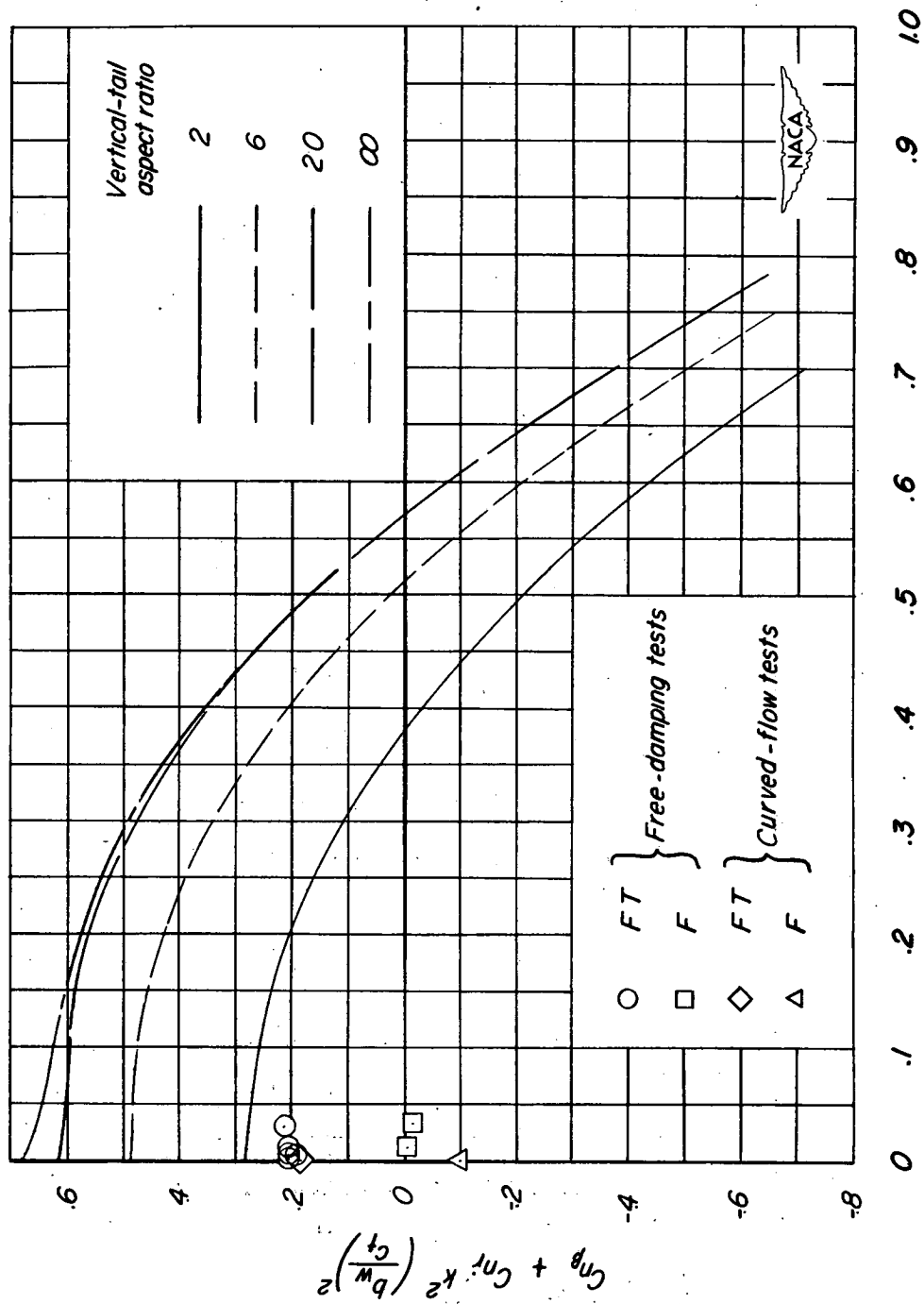

Figure 11.- The effect of aspect ratio on C_{n_β} as calculated by the method of Biot for a range of reduced frequencies.

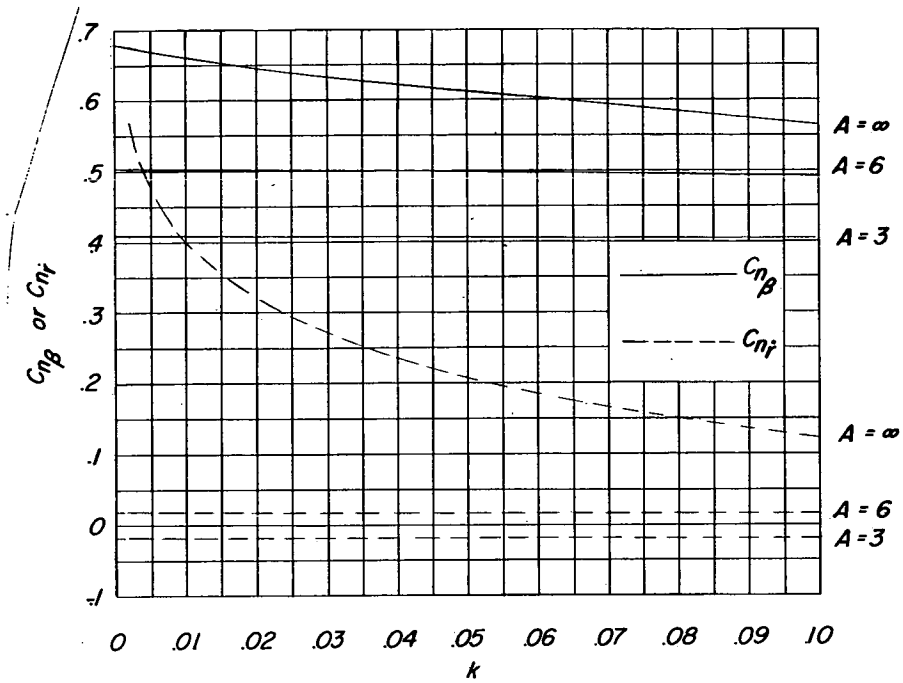

(a) Lower range of reduced frequencies.

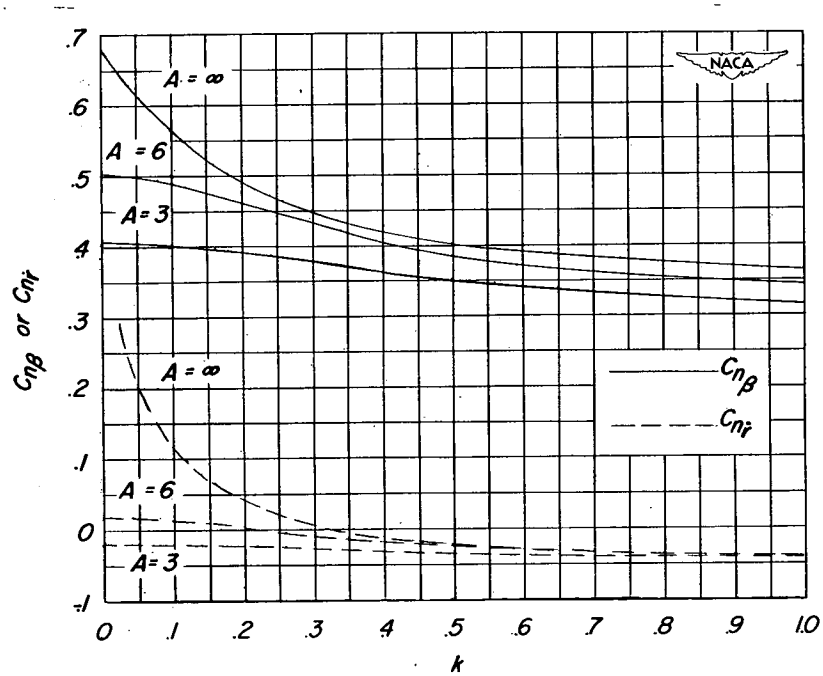

(b) Range of reduced frequencies.

Figure 12.- The effect of reduced frequency on the stability derivatives C_{n_β} and C_{n_r}.

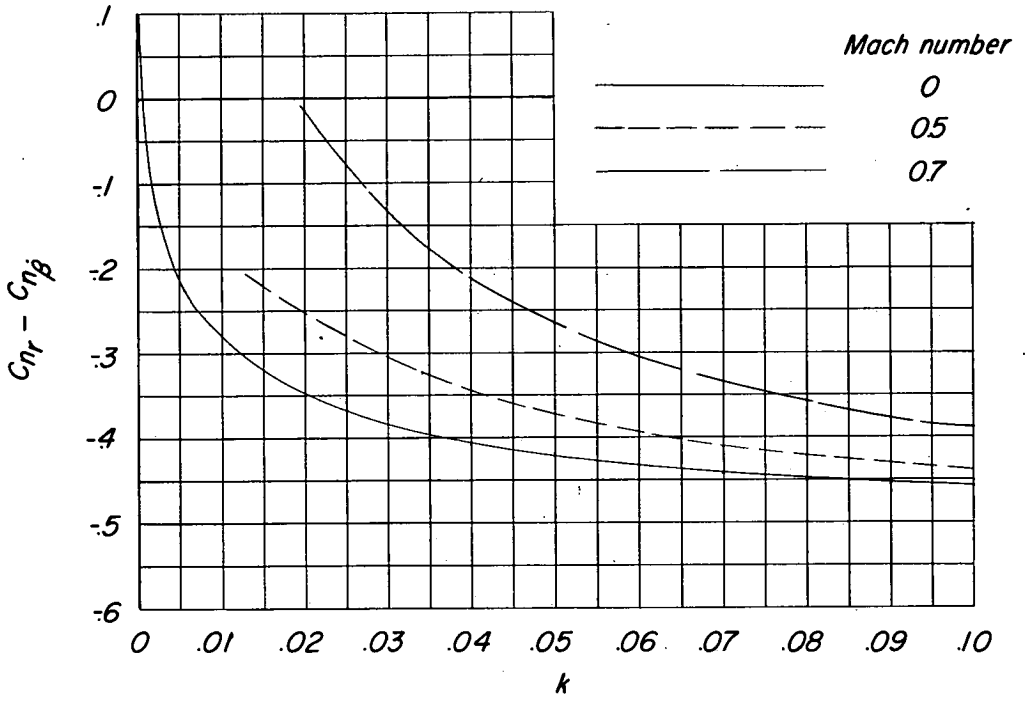

(a) Lower range of reduced frequencies.

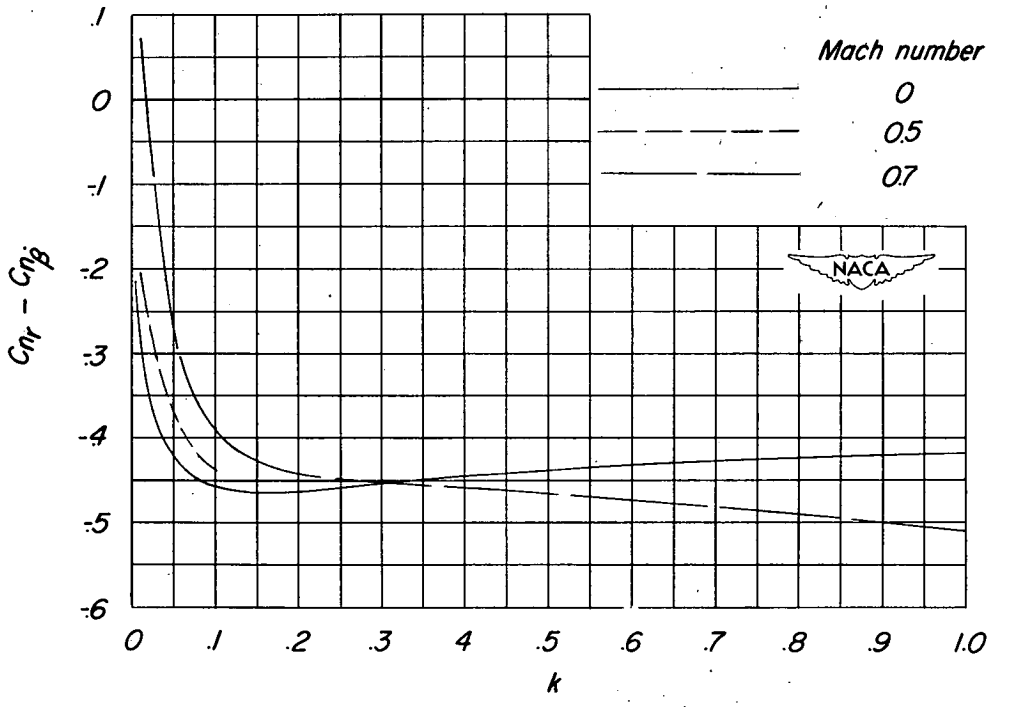

(b) Range of reduced frequencies.

Figure 13.- The effect of compressiblity on the damping in yaw.

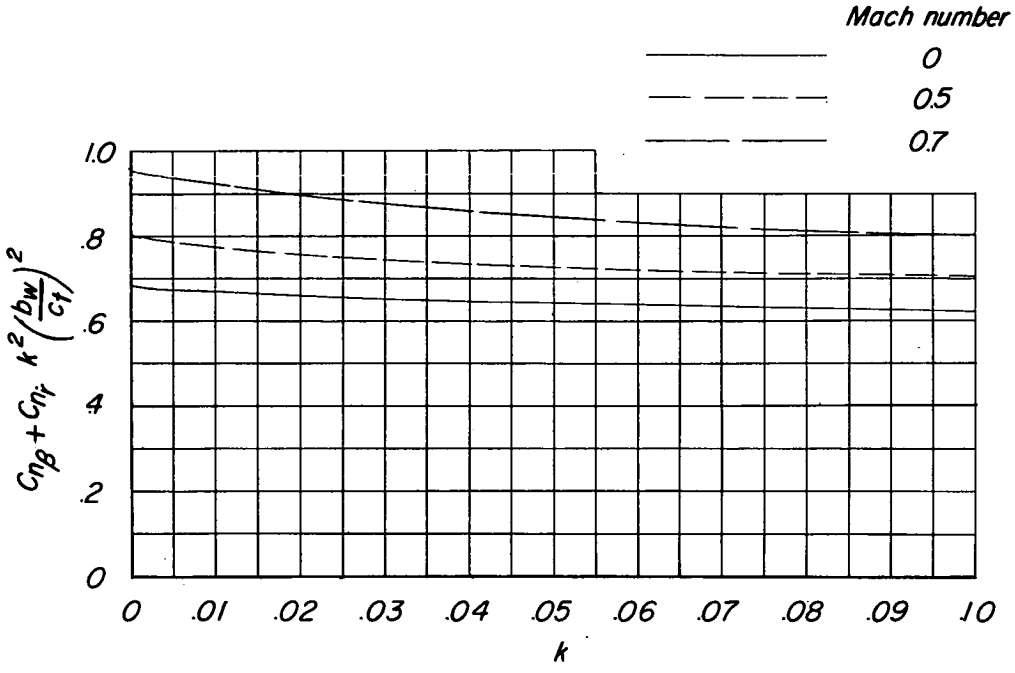

(a) Lower range of reduced frequencies.

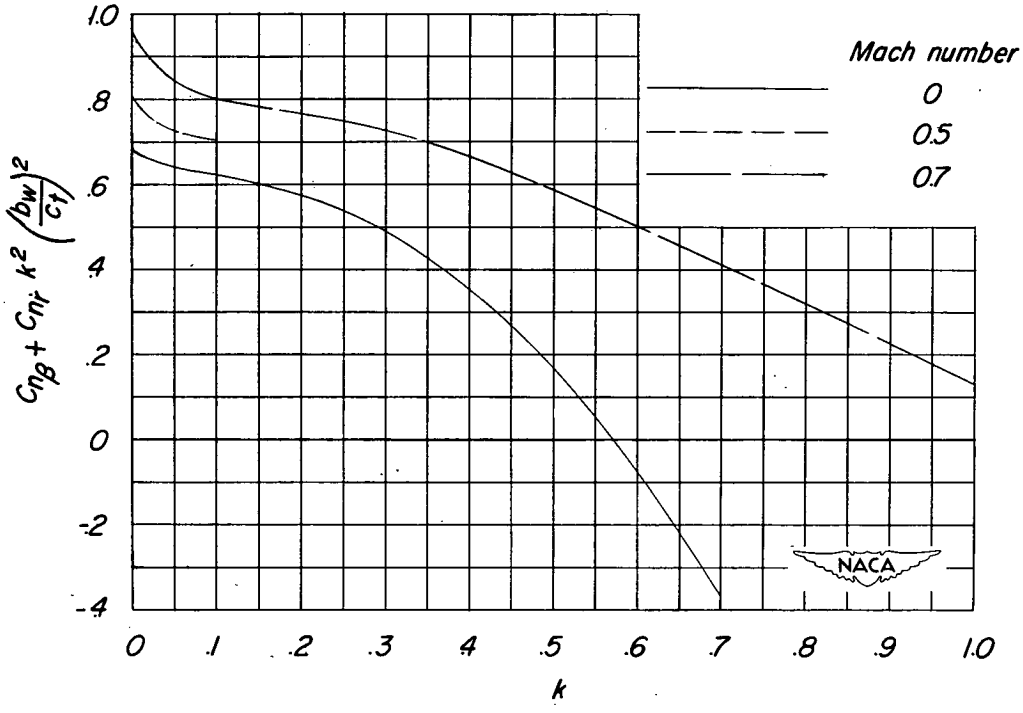

(b) Range of reduced frequencies.

Figure 14.- The effect of compressibility on the directional stability.

NACA-Langley - 4-15-52 - 1000